DOE/NV/11718--699

Simulations of liners and test objects for a new Atlas Advanced Radiography Source

Robert A. Hilko, Dane Morgan, and Steve Iversen, Bechtel Nevada (BN)

INTRODUCTION

Bechtel Nevada (BN) performed a computer modeling study to compare the proposed Atlas[1] Advanced Radiography Source (ARS) based on the rod-pinch concept[2, 3] with the current BN-Platts flash X-ray radiography[4] source. Los Alamos National Laboratory (LANL) Group DX-3 code BIE[5, 6] was used to generate synthetic radiographs of the Atlas liners and targets. A comparison of relevant X-ray source parameters appears in Table 1.

Table 1 – X-Ray Source Parameters

Source Feature	BN-Platts	Atlas ARS
Anode-Cathode diode	Tapered tungsten rod inside a cold emission cathode	Rod-pinch
X-ray endpoint	0.25 MeV(ref 7)	1.2 to 2.4 MeV
Source width, w_s	0.15 cm	0.075 cm (ref 3)
Dose at 1 meter	0.01 R	2 R
X-ray pulse width	10-20 ns (nanoseconds)	25 ns (ref 3)

The estimated X-ray endpoint of 1.5 MVp for the Atlas ARS had not been verified experimentally, and thus, an investigation with endpoint energies of 1.2, 1.8, 2.1, and 2.4 MVp was added. The Atlas ARS source width[3] was based on the use of a 0.05-cm-diameter tungsten anode rod.

METHOD

The BIE is an interactive code in which simulated images are created by connecting boxes on a computer screen canvas. Each box is called a *glyph* and performs a specific, defined function, such as 2-D convolution. In this computer simulation, an aluminum liner is included by requesting the geometry glyph, where two symmetrical rectangles equidistant apart are drawn. The *y* dimension is the height, and the *x* width becomes the cylindrical tube thickness. We then place this geometry onto a uniform grid, where the test-object spatial resolution is defined. The threshold glyph assures that no spurious values occur. The scaling glyph sets the actual material density. The conebeam on the axis glyph performs three sequential operations. It accepts the geometry information and rotates it about the y axis into a solid. It then performs projections based on the source-to-object distance, D, and object center-to-imaging detector distance, d. The line integral of the projected areal mass in units of grams per cm^2 is inserted into each newly defined imaging detector pixel. D equals 100 cm, and d is 39 cm, yielding a magnification, M, of 1.39. The newly defined image can be either the complete object or a definable portion. The BIE calls the newly defined image a detector. We then insert the material wrapper glyph to provide the mass attenuation coefficients as a function of X-ray energy. Geometries of the same material can be summed together. A similar pattern is conducted for each different material. The next glyph, called the beam spectrum exponential, performs the transmission weighted by detector efficiency summed over all X-ray energies in the beam spectrum input for each pixel. We input the detector efficiency during the setup of the beam spectrum exponential glyph, including the beam spectrum via a separate glyph. The detector efficiency is for a Lanex-type rare-earth doped gadolinium-oxysulfide (GSO) intensifying screen that converts the absorbed energy into light. The light exposes a Kodak min RH-type film. The weighted transmission is modified by a two-dimensional convolution glyph to simulate geometric unsharpness[8] due to the finite source size simulated by a 2-D, unity-normalized Gaussian of equally wide dimensions. The equation used to calculate source width blur, w_b, at the imaging detector is:

$w_b = w_s (M-1)$, where M is 1.39 calculated by (D+d)/D.

The glyph series following this 2-D convolution then relates the blurred imaging detector weighted transmission, T, to microdensitometry film density. For the BN-Platts simulation, the T value of unity is set to 3200, and the ARS value is set to 4000 to produce the radiographs. This is a very rough guess for the enhanced ARS output. A 1-D convolution (usually not included) simulates the motion blur of the simulated objects along the radial axis before the conebeam on the axis glyph.

Test Objects

Two test objects were studied. The first object is a friction experiment,[9] where an aluminum cylinder lies between two tantalum endcap cylinders. In the actual experiment, a series of lead wires are inserted into the aluminum as markers to measure how the aluminum moves radially inward after the aluminum liner impacts both the aluminum and tantalum cylinders. The movement of the lead wire is detected by an X-ray radiograph. For purposes of this study one lead wire is placed at the aluminum center. The lead diameter varies from 0.02 to 0.04 cm, in 0.005-cm increments. Initial measurements[9] have shown that at the aluminum tantalum interface, very turbulent changes affect the lead wires. A simple model known as series 5 creates a heavily distorted shape in the lead at the sliding interface,[10] as seen in Figure 1.

Figure 1. A simple view of the friction geometry is shown. Black = vacuum. Light grey = aluminum. Very light grey = lead wire with heavy distortion at the point of contact with tantalum endcaps (white).

The second object comes from the VNIIEF Atlas experimental proposal[11] known as Rus-6. The aluminum liner compresses a layer of polyethylene. Dynamic high pressures test the strength of the copper object, whose inner radius is 1.6 cm and outer radius is 1.8 + f(y), where f(y) are two different wavelength sinusoidal functions. The equation for f(y) where y is the dimension along the central axis of the cylinder is

$$f(y) = 0.04 \sin(2\pi y/ 0.04),\ y = -2 \text{ to } 0.6 \text{ cm},\quad f(y) = 0.04 \sin(2\pi y/ 0.02),\ y = 0.6 \text{ to } 1.8 \text{ cm}.$$

The aluminum liner inner radius is 2.9 cm; the outer radius is 3.1 cm. A polyethylene tube with minimum gaps fills the region between the liner and test object.

Figure 2. The Rus-6 simulated geometry through the center of the load without projection. Black= vacuum. White = copper test object with sinusoidal surface. Moving outward, dark gray = polyethylene, even darker gray = aluminum liner.

2-D resolution

The BN-Platts source blur is simulated to be 0.0585 cm FWHM and 0.029 cm FWHM in the ARS at the film. This corresponds to blurs of 0.045[12] cm and 0.0225 cm, respectively.

Film response curve

The film response curve is density in microdensitometry units versus logarithm of light exposure (see reference 8, page 218). As stated previously, this curve can only be applied after establishing the maximum density value from an unobstructed view of the radiographic source, which is estimated on the current Atlas test cell.

X-ray spectrum

The BN-Platts spectrum is similar to the one described in footnote 13. The ARS spectra were calculated via MCNPX.[14] The MCNPX modeling of the ARS spectra used a 0.05-cm-diameter tungsten rod with the electrons impinging perpendicularly at the last 0.2 cm. The unattenuated total X-ray-per-electron predictions for five spectra were 5.4 e-7, 7.5 e-7, 1.0 e-6, 1.2 e-6, and 1.5 e-6, for the five MVp values in increasing value. The spectra were attenuated by 1.0 cm of aluminum return conductor, 3.105 cm of high-density polyethylene (HDPE), and 0.635 cm of Lexan. The HDPE and Lexan are flat blast shields for the intensified film pack. For purposes of this computer study, the X-ray properties of Lucite were used as a reasonable substitute for the Lexan. The return conductor is modeled as a flat attenuator in order to maintain spatial resolution. The spectra were unit-normalized before the attenuation factor was determined. Figure 3 shows the attenuated BN-Platts and attenuated, MCNPX-predicted, 1.5-MVp spectra. Attenuation factors were 0.20 and 0.46, respectively.

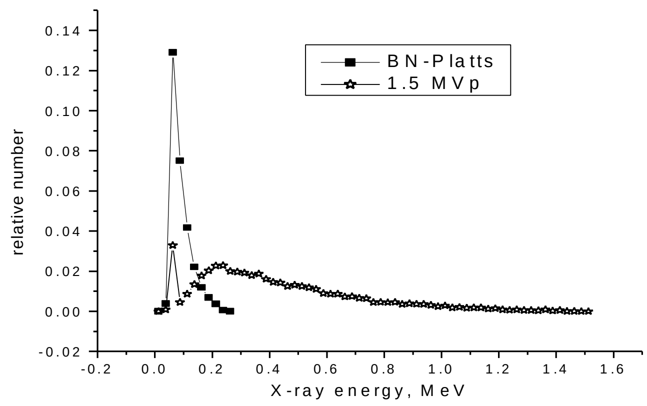

Figure 3. BN-Platts[13] and MCNPX 1.5-MVp unity-normalized spectra attenuated by the blast shield and aluminum return conductor.

The other four MCNPX spectra were similar, following the trend seen in the 1.5-MVp spectra in Figure 3, where the prominent 0.060-MeV and 0.250-MeV peaks decreased as the electron MVp value increased.

Imaging detector efficiency

The BIE imaging detector efficiency is the amount of energy deposited in the intensifying screen or scintillator for an X ray. The Lanex (rare-earth doped gadolinium oxysulfide, or GSO, material) intensifying screen efficiency had been previously extended to 0.25 MeV.[15] For the ARS simulation, this must extend to at least 2.4 MeV. Initially we used the mass-absorption coefficients for GSO provided on the NIST Web site.[16] However, MCNPX tests revealed that this premise overestimated the amount of absorbed energy for the 0.015-cm-estimated-thickness material, and that a thickness of 0.020 cm more closely matched the earlier work. It is assumed that the blast shield material was not equilibrating the X-ray beam. Figure 4 displays the two results. Since it is best to be conservative when simulating, we used the MCNPX extended efficiency curve.

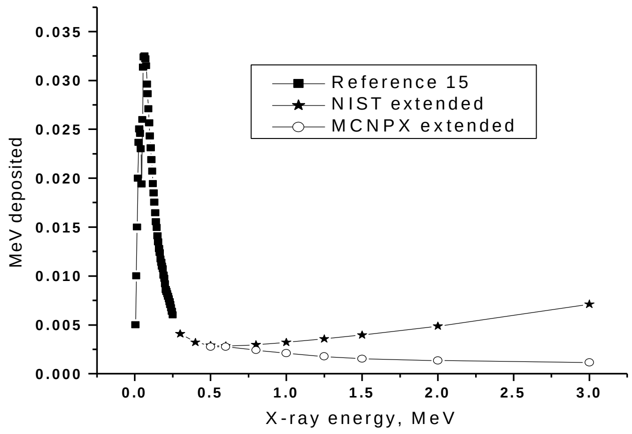

Figure 4. Lanex intensifying screen energy deposited as a function of X-ray energy. The curve with block designator is from reference 15. The stars and open circles are the results of extending this earlier work to higher energy.

SIMULATIONS

Motion blur

As stated earlier, convolving with a blurring function before the conebeam projection and line integrals function can include motion blur. The maximum liner velocity, per reference 1, is 2.2 cm/microseconds. A simple analysis to assess expected motion blur appears in Table 2, below. The object displacement is scaled by magnification and assumes that the X-ray pulse time profile is Gaussian. Due to the smaller source size of the ARS, motion blur could be detectable starting at 0.7 cm/μs, while motion blur may be undetectable with the BN-Platts source.

Table 2 - Predicted Blur (FWHM, cm) from Motion and Source

	Motion Blur		**Total Blur**	
Material velocity, cm/microseconds, ms	**BN-Platts cm**	**ARS cm**	**BN-Platts cm**	**ARS cm**
0.1	0.001	0.0025	0.0585	0.0291
0.5	0.005	0.0125	0.0587	0.0316
0.7	0.007	0.0175	0.0589	0.0339
1.0	0.010	0.0250	0.0593	0.0383
2.2	0.022	0.0550	0.0625	0.0622

Test object 1

Test object 1, series 5 option, source-blurred simulations are shown in Figure 5.

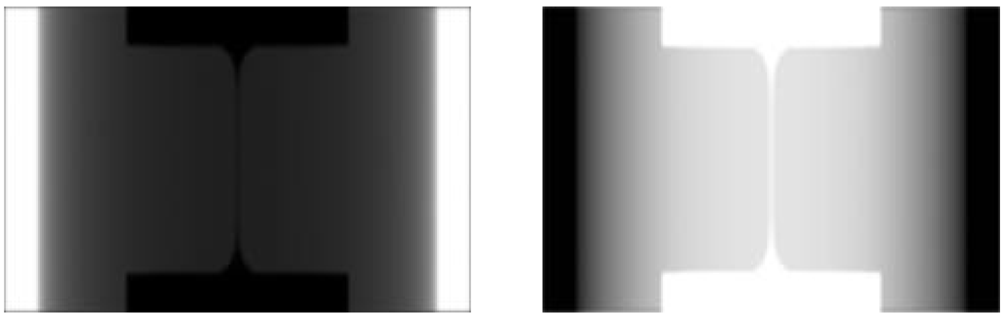

Using BN-Platts source,
transmission-weighted image

Using BN-Platts source,
simulated film image

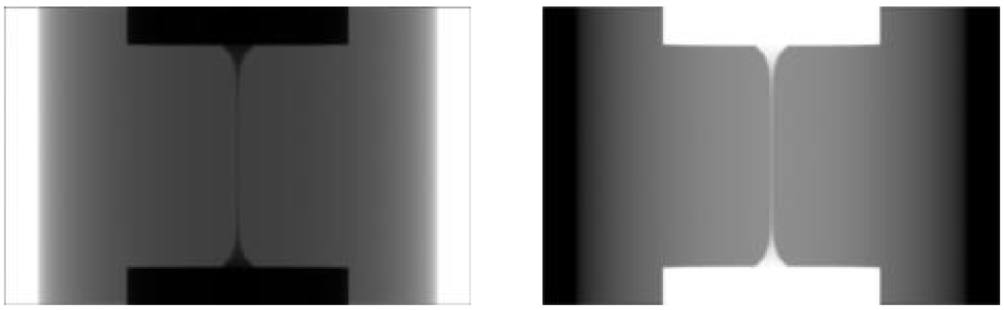

Using Atlas ARS, 1.5-MVp
Transmission-weighted image

Using Atlas ARS, 1.5-MVp
simulated film image

Figure 5. Simulated images of test object 1 with option series 5

Row plots were done across the region in which the lead wire was located for BN-Platts and the five different ARS spectra. The results of analyzing the weighted transmission difference, ΔT, and lead wire width are summarized in Table 3. 1.2-MVp, 2.1-MVp, and 2.4-MVp results were similar to the 1.5-MVp case.

Table 3 – Row Plot Results

Wire diameter, cm	Source	DT	Width, cm
0.020	BN-Platts	0.0227	0.0579
0.020	1.5 MVp	0.0352	0.0306
0.025	BN-Platts	0.0338	0.0626
0.025	1.5 MVp	0.0469	0.0358
0.030	BN-Platts	0.0425	0.0631
0.030	1.5 MVp	0.0600	0.0377
0.035	BN-Platts	0.0537	0.0665
0.035	1.5 MVp	0.0710	0.0437
0.040	BN-Platts	0.0604	0.0677
0.040	1.5 MVp	0.0775	0.0477

The resolution appears to be sufficient for all, but the ARS provides better contrast. Here we assume that the film is exposed properly and that the criterion for detectability is that ΔT is greater than 0.02 to appear above background noise.

Figure 6 shows tests of the detectability of the lead next to the tantalum. The columns were compared to quantify what could be seen through the tantalum endcaps of test object 1. Even the highest energy simulation tested predicted 1% transmission, which really cannot be considered detectable. The ARS better discriminates the simulated, distorted shape of the lead at the tantalum interface for all MVp values.

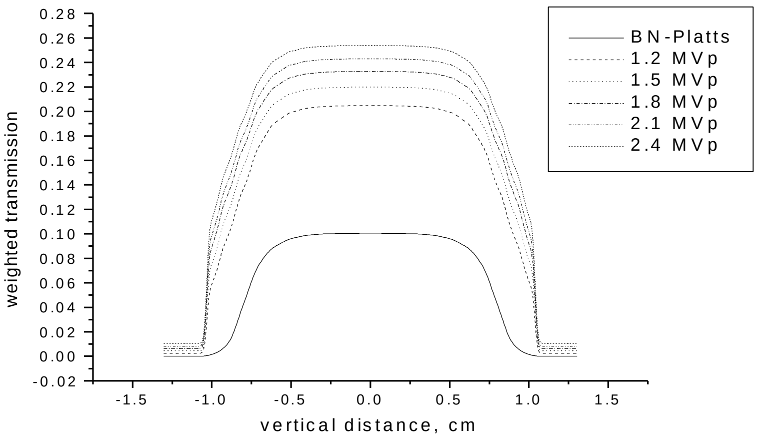

Figure 6. Test object 1 column profiles through the lead series 5 option wire for all X-ray spectra

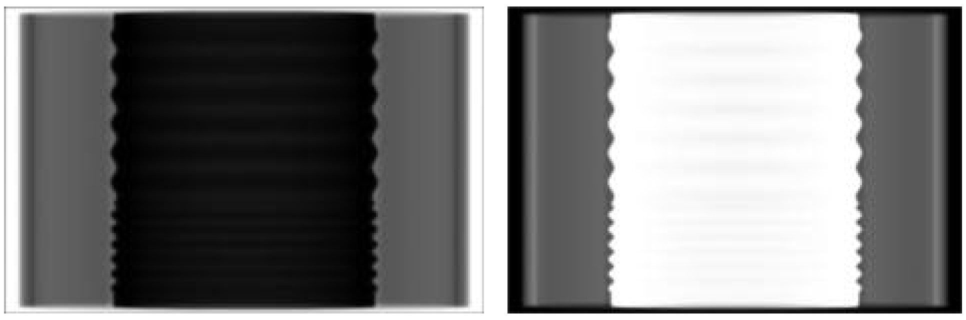

Using BN-Platts source, transmission-weighted image

Using BN-Platts source, simulated film image

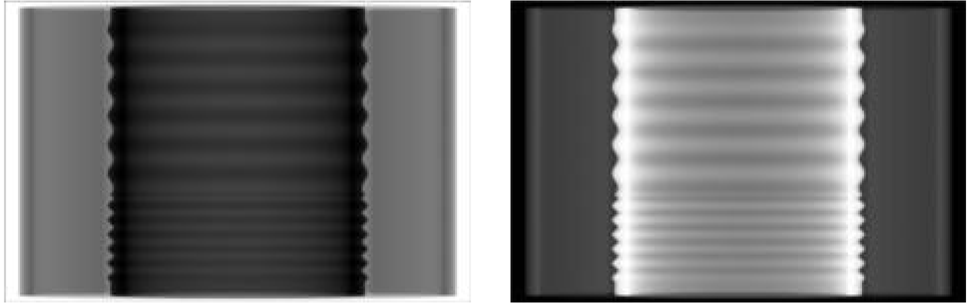

Using Atlas ARS, 1.5-MVp transmission-weighted image

Using Atlas ARS, 1.5-MVp simulated film image

Figure 7. Simulated transmission-weighted and film images of test object 2, Rus-6

In the real experiment, we plan to measure the growth of the tips relative to the inside radius. From the simulated images, line profiles were created through the tips and valleys of the perturbations for the transmission-weighted images, for both BN-Platts and ARS 1.5-MVp simulations (see Figure 8).

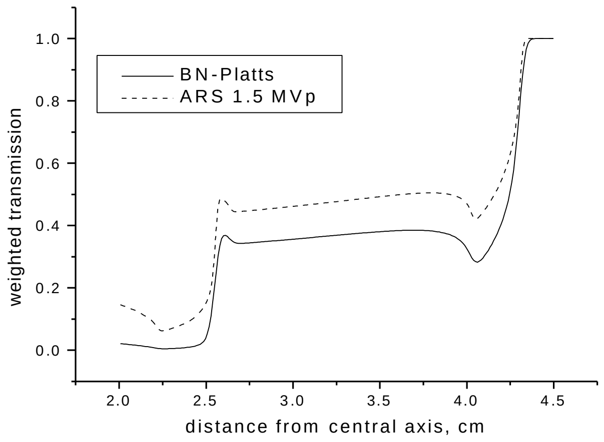

Figure 8. Line profiles compared through the small wavelength tip of the weighted transmission simulated film images of test object 2, Rus-6, for the current BN-Platts and the ARS 1.5-MVp X-ray source. Source blur is included.

The copper's inside edge is at about 2.25 cm and is clearly identifiable with the ARS simulation, while for the BN-Platts, the weighted transmission is at 1%, which is not detectable. The tip region at 2.6 cm is sharper with the BN-Platts because the X rays could not penetrate the copper.

Radially outward, there is a small air gap, then the polyethylene. Finally, after 4.0 cm, the simulated aluminum liner is discernable with either source. Because it can penetrate the copper, the ARS proves superior.

CONCLUSIONS

The Advanced Radiographic Source will improve the data significantly due to its smaller source width. Because of the enhanced ARS output, larger source-to-object distances are a reality. The harder ARS source will allow radiography of thick high-Z targets. The five different spectral simulations resulted in similar imaging detector weighted transmission. This work used a limited set of test objects and imaging detectors. Other test objects and imaging detectors could possibly change the MVp-sensitivity result. The effect of material motion blur must be considered for the ARS due to the expected smaller X-ray source size. This study supports the original 1.5-MVp value.

REFERENCES

[1] W. M. Parsons *et al*., "The Atlas Project: A new pulsed power facility for high energy density physics experiments," IEEE Trans. Plasma Sci. **25**, 205-211 (1997).
[2] R. A. Mahaffey, J. Golden, S. A. Goldstein, and G. Cooperstein, "Intense electron-beam pinch formation and propagation in rod-pinch diodes," App. Phys. Lett. **33**, 795–797 (1978).
[3] P. R. Menge *et al.*, "Rod-pinch radiography source optimization at 2.3 MV," in *IEEE Conference Record Abstracts* (Pulsed Power Plasma Science 2001, 28th IEEE International Conference on Plasma Sciences and 13th IEEE International Pulsed Power Conference, Piscataway, NJ), pp. 454–457.
[4] D. Platts, M. P. Hockdaday, D. Beck, W. Coulter, R. C. Smith, "Compact flash X-ray units," *Proc. IEEE-IPPC '95*, 892–897 (1995).
[5] G. S. Cunningham, K. M. Hanson, G. R. Jennings Jr., and D. R. Wolf, "An interactive tool for Bayesian inference," Rev. of Prog. Quan. Nondestructive Eval. **14A**, 747-754 (2000).
[6] K. M. Hanson and G. S. Cunningham, "A computational approach to Bayesian inference," Comput. Sci. & Stats. **27**, 202–211 (1996).
[7] D. V. Morgan, D. Platts, J. S. Shlacter, D. L. Martinez, B. Carpenter, "Analysis of radial radiography for the liner stability series at Pegasus: PGII-59, PGII-62, and PGII-63," *Proc. IEEE-IPPC '97*, pp. 1381–1386.
[8] Michel M. Ter-Pogossian, *The Physical Aspects of Diagnostic Radiology*, 1st ed. (Harper & Row, Hagerstown, MD, 1967), p. 283.
[9] J.E. Hammerberg *et al.*, "A Pegasus dynamic liner friction experiment," *Shock Compression of Condensed Matter-1999*, edited by M. D. Furnish, L. C. Chabildas, and R. S. Hixson (American Institute of Physics, Melville, NY, 2000), pp. 1217–1220.
[10] J. Hammerberg (private communication).
[11] A. M. Buyko, V. N. Mokhov, P. N. Nitzovtsev, V. P. Solovyev, and V. B. Yakubov, "Physical schemes of liner units for the experiments on capacitor bank Atlas (Rus-6,7,8)," Russian Federal Nuclear Center–All-Russian Research Institute of Experimental Physics, Sarov, Russia, 2001 (unpublished).
[12] J. Ladish (private communication).
[13] Hewlett Packard Technical Bulletin B-23 (unpublished).
[14] H. G. Hughes, R. E. Prael, and R. C. Little, "MCNPX—The LAHET/MCNP code merger," LANL Research Note XTM-RN(U)97-012, April 22, 1997.
[15] S. L. Issler and C. C. Torardi, "Solid state chemistry and luminescence of X-ray phosphors," J. Alloys Compounds **229**, 54–65 (1995).
[16] National Institute of Standards and Technology (NIST) Web site, www.physics.nist.gov.

DISCLAIMER

DISTRIBUTION LIST

U.S. Department of Energy
National Nuclear Security Administration
Nevada Operations Office
P.O. Box 98518
Las Vegas, NV 89193-8518

U.S. Department of Energy
Office of Scientific and Technical Information
P.O. Box 62
Oak Ridge, TN 37831
(electronic copy)

DOE/NNSA
Public Reading Facility
P.O. Box 98521
Las Vegas, NV,
89193-8518